

PREPARATION OF Al₂O₃/TiO₂ NANOCOMPOSITES FOR HUMIDITY SENSING APPLICATIONS

V. RAJENDAR^{a,c}, T. SOWMYA^b, K. V. RAO^b, B. POORNAPRAKASH^c,
M. KUMAR^a, S. H. PARK^{a*}

^a*Department of Electronics Engineering, College of Engineering, Yeungnam University, Republic Korea.*

^b*Centre for Nano Science and Technology, Jawaharlal Nehru Technological University Hyderabad, India.*

^c*Department of Physics, B.V. Raju Institute of Technology, Narsapur, Medak, Telangana, India*

Highly porous Al₂O₃/TiO₂ nanocomposites were prepared by the co-precipitation method. The nanocomposites calcined at 800°C showed characteristic peaks during structural analysis with an average crystallite size of 25nm. The particle size was estimated to be in the range of 15nm through transmission electron microscopy. The band gap of the materials was calculated by analyzing the UV spectra and showed a red shift with a decrease in the direct band gap to 2.8 eV. The nanocomposites showed an increase in their resistivity and porosity with increasing Al₂O₃ concentration. These parameters accompanied by their lower density show that Al₂O₃/TiO₂ nanocomposites are suitable candidates for humidity sensor applications.

(Received August 15, 2016; Accepted October 13, 2016)

Keywords: Al₂O₃/TiO₂ nanocomposites; humidity sensor; co-precipitation;

1. Introduction

Nanotechnology and nanomaterials are currently dominating every field of science by disrupting conventional methods of application (1-7). They have been used for solar cell(8-9), antibacterial(10, 1) and light harvesting applications(11) to name a few. In the past decade, significant advances have been made in the field of sensors owing to the wide spread use of nanotechnology and nanomaterials (12-15). In this respect, the introduction of gas sensors, which need the highest sensitivity, has paved the way to the development of the most advanced nanoscale sensors (16-17). This, in-turn, has resulted in the advancement of sensing technologies in the field of humidity sensing (18-19), effluent sensing (20-23) and even bio-sensing (24). Of these, humidity sensors have seen the greatest progress owing to their use in the semiconductor industry, where moisture or humidity values need to be continuously monitored. Furthermore, their use in domestic applications including air-conditioners and microwaves and commercial applications, such as greenhouse filters, respiratory equipment, etc., has necessitated the production of low cost, highly efficient humidity sensors (25-27).

Humidity sensors can be divided into two major types depending on whether they measure the relative or absolute humidity. Of these, relative humidity sensors have been fabricated using ceramics, semiconducting materials and polymers. Absolute humidity sensors, which measure the exact amount of water/kilogram of air, have been conventionally made using mirror based hygrometers. However, porous aluminum oxide (Al₂O₃) thin-film sensors have also been used for the measurement of the absolute humidity. Many recent reviews quote the use of Al₂O₃ sensors integrated and impregnated with other materials for the sensing of the humidity at the ppm (parts per million) and ppb (parts per billion) level. Al₂O₃ sensors are typically built on an equivalent

* Corresponding author: sihyun_park@ynu.ac.kr

electric circuit model, where the sensor is represented by a parallel capacitance and resistance. However, due to the irreversible change from $\gamma\text{-Al}_2\text{O}_3$ to $\gamma\text{-Al}_2\text{O}_3\cdot\text{H}_2\text{O}$ under high humidity conditions, these sensors lose their sensitivity over time and need to be re-calibrated. To overcome this problem, $\gamma\text{-Al}_2\text{O}_3$ sensors are often coated with other hygroscopic materials such as NaCl, SnO_2 , TiO_2 etc. Of these materials, TiO_2 is the most promising candidate owing to its resistance based relative humidity sensing abilities.

In this paper, we discuss the preparation, characterization, mixing and humidity sensing abilities of a TiO_2 and Al_2O_3 nanocomposite. Three different mixtures were prepared with varying concentrations of individual nanoparticles in order to investigate the role of the mixing ratio in the behavior of the nanocomposite. The change in resistivity with increasing density and porosity reveal their candidature for humidity sensing applications.

2. Materials and methods

Aluminum nitrate nonahydrate ($\text{Al}(\text{NO}_3)_3\cdot 9\text{H}_2\text{O}$) (E.Merck (India) limited Co.), Sodium Hydroxide (NaOH; Thomas Bakers; 97.5%), Titanium dioxide (TiO_2 ; Accord Labs; 98%) and Polyvinyl Alcohol (PVA; HIMEDIA) were used in the synthesis of the materials. Distilled Water was used as the solvent for all of the synthesis processes.

Preparation Al_2O_3 and TiO_2 nanoparticles

Al_2O_3 and TiO_2 were prepared individually by the co-precipitation method. In a typical synthesis process, a 2 M NaOH solution was added dropwise to a 0.1 M precursor solution till the pH of the solution reached 10. The solution was stirred vigorously for one hour before filtering and washing the residue with distilled water multiple times. Post synthesis, the particles were dried and annealed at 800°C for 2 hours and allowed to cool to room temperature naturally. A small portion of the thus obtained powders were segregated for further analysis, while rest of the samples were used for the preparation of the nanocomposite.

Preparation of $\text{Al}_2\text{O}_3/\text{TiO}_2$ nanocomposite

The nanoparticles consisting of Al_2O_3 and TiO_2 were mixed at three different ratios with increasing amounts of Al_2O_3 (Table 1). All three mixtures were individually milled using a mortar and pestle for 4 hours before annealing them at 800°C for 2 hours.

Table 1: The ratio of Al_2O_3 and TiO_2 added to the mixture to make the nanocomposites

Mixture name	Al_2O_3 (x) (wt %)	$\text{TiO}_2(1-x)$ (wt %)
Composite 1	30	70
Composite 2	60	40
Composite 3	90	10

The annealed mixtures were mixed with a few drops of 3% PVA and then compressed into 50 mm pellets using a hydraulic press (KBr Press) for a period of 30 s under a pressure of 10 tons. The green colored pellets were then sintered at 650°C for 1 hour in order to remove the binder. The thus prepared pellets were utilized for further characterization and resistivity measurements.

3. Characterization

The structural analysis of the samples was conducted by an X-ray Diffraction (XRD) system (Bruker AXS D8 Advance) using $\text{CuK}\alpha$ radiation ($\lambda=1.5418 \text{ \AA}$) with an accelerating voltage of 40KV at 2 theta values in the range from 20° to 80° . The crystallite size of the samples was calculated by the Debye – Scherer formula. The morphology of the samples was studied by both transmission electron microscopy (TEM) and scanning electron microscopy (SEM). The UV

spectra of the samples were generated by a UV-Visible double-beam spectrophotometer (Lab India 2202) and used to calculate their band gap. Thermo gravimetric analysis was conducted on 20mg samples, in order to study the decomposition of PVA, and the formation of porous nanocomposites was conducted by an EXSTAR 6300R by heating the samples at a scan rate of 10°C/minute to 800°C for Al_2O_3 and 1000°C for TiO_2 . The resistivity measurements were carried out by means of custom-built I-V equipment using the 4-point probe method.

4. Results and discussion

The XRD analysis of the individual nanoparticles revealed the characteristic peaks for Al_2O_3 and TiO_2 matching JCPDS#88-0107 and JCPDS#86-1157, respectively. Al_2O_3 formed orthorhombic crystals with an average crystallite size of 21.4 nm and TiO_2 formed a stable Anatase phase with an average crystallite size of 29.4 nm. Figure 1 shows a combined graph of all of the samples including the composites. As expected, we observed an increase in the Al_2O_3 orthorhombic peak intensity with increasing Al_2O_3 concentration in the nanocomposites.

The morphology of the samples was predominantly spherical in shape with the agglomeration of small nano particles, as seen in the SEM images. The TEM images show much clearer square shaped and random shaped nanoparticles in the size range of 15 nm. While TiO_2 was spherical in shape, the Al_2O_3 sample contained predominantly square shaped nanoparticles.

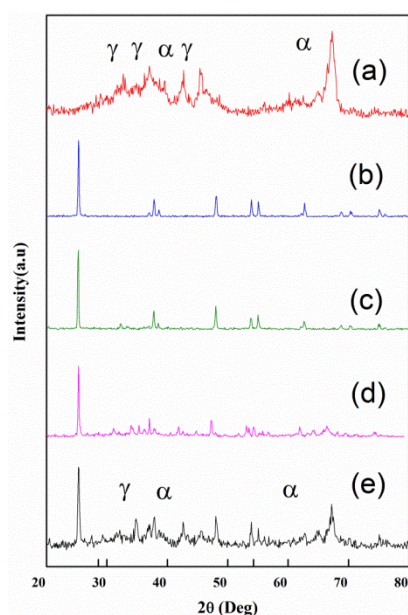


Figure 1: XRD diffractograms of all of the samples (a) Aluminum Oxide (b) Titanium Dioxide (c) Composite 1 (d) Composite 2 and (e) Composite 3. α represents the characteristic alumina orthorhombic phase, while γ represents Anatase phase.

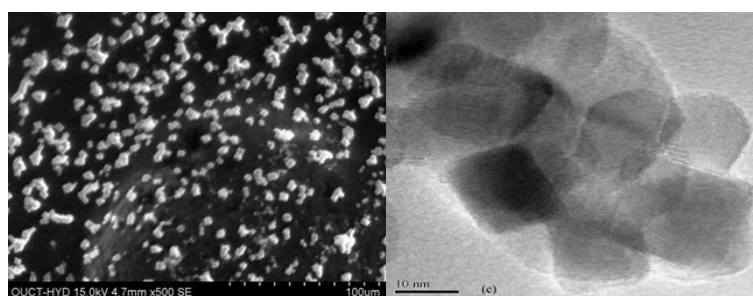


Fig. 2a: Al_2O_3 SEM and TEM Images

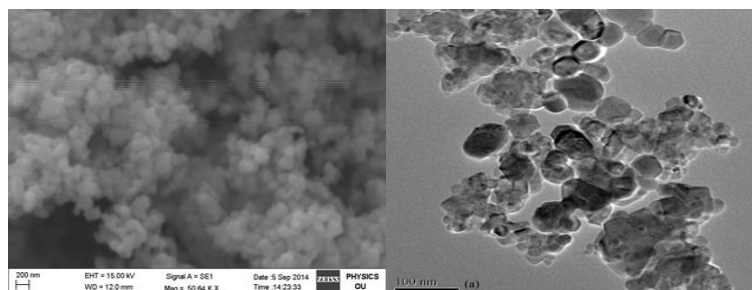


Fig. 2b: TiO_2 SEM and TEM Images

A systematic UV-visible optical absorption study was conducted on all of the samples. Figure 3 shows the Tauc plot of $(\alpha h\nu)^2$ versus the photon energy ($h\nu$) and extra plot of the linear portion of the absorption edge to find the intercept with the energy axis for the Al_2O_3 , TiO_2 and $\text{Al}_2\text{O}_3/\text{TiO}_2$ composites with different weight percentages. A significant broadening of the absorption edge was observed in case of the Al_2O_3 , TiO_2 and $\text{Al}_2\text{O}_3/\text{TiO}_2$ composites, which may be due to the inhomogeneous size distribution of the nanoparticles. The band gaps of the Al_2O_3 , TiO_2 and $\text{Al}_2\text{O}_3/\text{TiO}_2$ composites were calculated from the Tauc plots. The estimated band gap energies are 3.7 eV, 3.8 eV and for composites it is about 3.8 eV, 3.4 eV and 2.8 eV respectively.

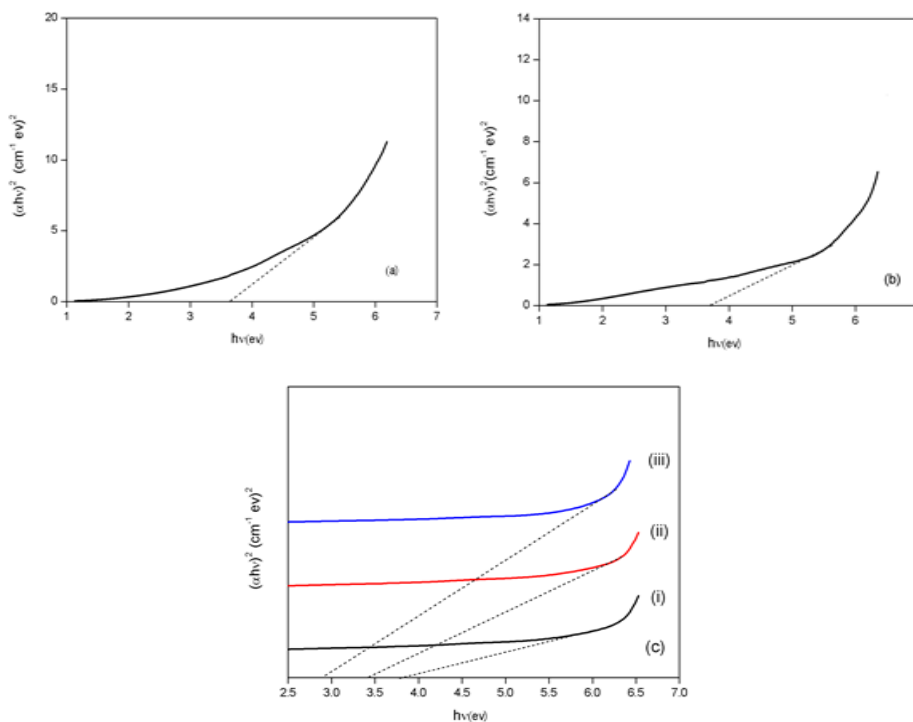


Fig. 3: Band energy of (a) Al_2O_3 material (b) TiO_2 material and (c) $\text{Al}_2\text{O}_3/\text{TiO}_2$ Nanocomposite with different weight percentages.

The thermogravimetric analysis and differential thermal analysis (TGA-DTA) of the samples showed characteristic biphasic and monophasic curves for Al_2O_3 and TiO_2 , respectively. As these tests were conducted to confirm the composition of the samples, the characteristic curves were compared with those of the nanocomposites. As expected, the composites showed a monophasic weight loss pattern at higher concentrations of TiO_2 and subsequently followed a biphasic weight loss pattern for composites 2 and 3. The biphasic weight loss can be attributed to the transition of Aluminum hydroxide to boehmite at 195°C followed by a phase transition into

orthorhombic Al_2O_3 at 350°C . It can be inferred based on the absence of any additional unexpected peaks appearing during the analysis that the samples contained no impurities. All of the results from the TGA-DTA analysis can be seen in figure 4. In figure 4(a), the initial stage of weight loss is from 150 to 280°C and the last stage of weight loss is from 280 to 650°C . In figure 5.9 (b), the weight loss occurs from 550 - 800°C .

Ed. - Highlight - Please verify/clarify the technical meaning.

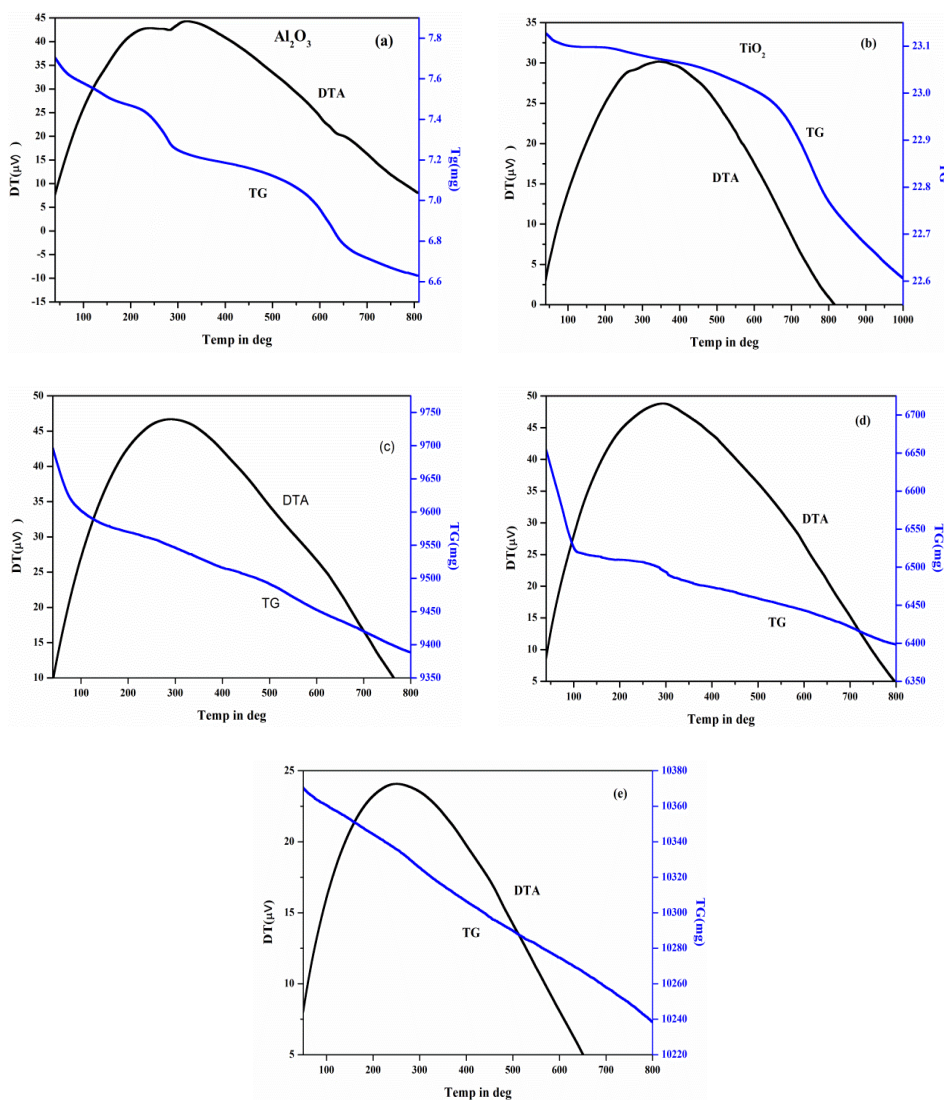


Fig. 4: TG-DTA (a) Al_2O_3 material, (b) TiO_2 material (c), nanocomposite, (d) nanocomposite 2 and (e) nanocomposite 3.

Density and Porosity measurements

Theoretically, the density (ρ^{th}) of the samples can be analyzed based on the weight and volume they occupy. However, in reality, the true density (ρ^{m}) of the material varies from its theoretical value. The porous nature of the material, responsible for this difference, can be measured as a function of the ρ^{m} percentage relative to ρ^{th} . Figure 5 portrays the measured density and calculated porosity of the samples. It is evident that with increasing Al_2O_3 concentration, the porosity of the composites increases, while their density decreases.

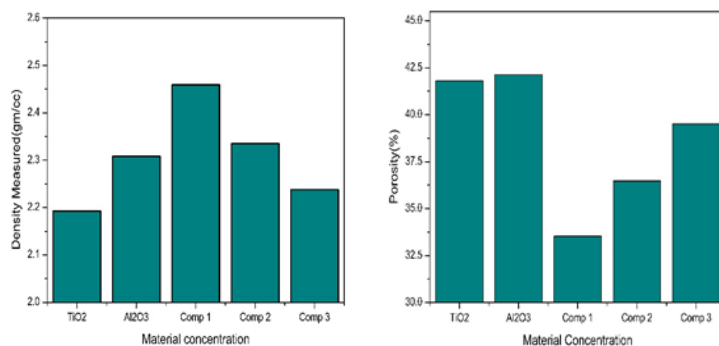
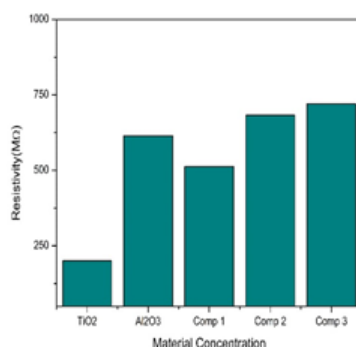


Fig.5:(a) Graph of Material Concentration versus Measured Density (b) Graph of Material Concentration versus Porosity (%).

Resistivity Measurements

The resistivity measurements for all of the samples were performed using a custom-built IV setup using a 4-point method. Figure 6 shows the resultant resistivity values for all of the samples at room temperature. The TiO₂ samples showed the lowest resistivity values as compared to all the other samples, while composite 3 showed the highest resistivity. TiO₂ had the resistivity of 200.876 MΩ, followed by composite 1 (512.461 MΩ), Al₂O₃ (614.380 MΩ), composite 2 (683.281 MΩ), and composite 3 (720.465 MΩ). The resistivities of all of the samples designed for humidity sensing applications were higher than those of the materials.



Fi.e 5.11: Resistivity versus Material Concentration graph

4. Conclusions

Al₂O₃ and TiO₂ nanoparticles were prepared through the co-precipitation method. Three different mixtures with varying concentrations of Al₂O₃ were used for the preparation of nanocomposite pellets. All of the samples were heated at 800°C in order to form crystalline phases and contain edno impurities. The density and porosity measurements showed an increase in the porosity of the composites with increasing Al₂O₃ concentration. An increase in the resistivity values was observed, which confirmed that the composites were ideal candidates for humidity sensing applications.

Acknowledgment

The authors are grateful to the department of Electrical Engineering, Yeungnam University, Republic of Korea and the Centre for Nano Science & Technology, Jawaharlal Nehru Technological University, Hyderabad, India, for providing the research facilities to undertake this work.

References

- [1] V. Rajendar, B. Rajitha, T. Dayakar, CH. Shilpa Chakra, K. Venkateswara Rao, *Rend. Fis. Acc. Lincei*, Accepted, DOI 10.1007/s12210-016-0511-0.
- [2] P. Alivisatos, *Nat Biotechnol.* **22**(1),47 (2004).
- [3] M. Daniel, D. Astruc, *Chem Rev*, **104**(1),293 (2004).
- [4] M. Ferrari, *Nat Rev Cancer*, **5**(3),161 (2005).
- [5] D. Li, Y. Xia, *Adv Mater*, **16**(4),1151 (2004).
- [6] G. Oberdorster, E. Oberdorster, J. Oberdorster, *Environ Health Perspect*, **113**(7) 823 (2005).
- [7] D. Peer, J.M. Karp, S. Hong, O.C. Farokhzad, R. Margalit, R. Langer, *Nat Nanotechnol*, **2**(12),751 (2007).
- [8] PV. Kamat, *J PhysChem C*, **112**(48,18737 (2008).
- [9] M.Gratzel, *AccChem Res*, **42**(11),1788 (2009).
- [10] V. Rajendar, T. Dayakar, K. Shobhan, I. Srikanth, K. Venkateswara Rao, *SuperlatticesMicrostruct.***75**,551 (2014).
- [11] V.Rajendar, B. Rajitha, K. Venkateswara Rao, *J Mater Sci Mater Electron*, **26**(12), 9661 (2015).
- [12] AK. Akhnoukh, *Micro Nanosystems*, **5**(2),147 (2013).
- [13] N. Invernizzi , *J Nanopart Res*, **13**(6),2249 (2011).
- [14] K.Y. Kim, *NanomedNanotechnolBiol Med*, **3** (2) (2007).
- [15] Y. Oh, K. Kim, S. Hwang, H. Ahn, J. Oh, J. Choi, *ApplSpectrosc Rev*, **51**(7-9),656 (2016).
- [16] R. Hajihashemi, A.M. Rashidi, M. Alaie, R. Mohammadzadeh, N. Izadi, *Mater SciEng C*, **55**, 417 (2014).
- [17] K.J. Huang, *Advanced Materials Research*, **159**,634 (2011).
- [18] H. Lee, S. Lee, S. Jung, J. Lee, *B Chem*, **154**(1),2 (2011) .
- [19] K. Jaruwongrungrsee, A. Tuantranont, Y. Wanna, A. Wisitsoraat, T. Lomas, 2007 7th IEEE International Conference on Nanotechnology - IEEE-NANO 2007, Proceedings.
- [20] Z. Gao, W. Li, B. Liu, F. Liang, H. He, S. Yang, C. Sun, *J Chromatogr A*, **1218**(37),6285 (2011).
- [21] SK. Brar, M. Verma, R.D. Tyagi, R.Y. Surampalli, *Waste Manage*, **30**(3),504 (2010) -20.
- [22] S. Chakraborty, M.K. Purkait, S. DasGupta, S. De, J.K. Basu, *Sep PurifTechnol*, **31**,141 (2003) .
- [23] F. Gottschalk, T. Sun, B. Nowack, *Environ Pollut*, **181**,287 (2013).
- [24] A. Salimi, A. Noorbakhash, E. Sharifi, A. Semnani, *BiosensBioelectron*, **24**(4) 792 (2008) .
- [25] Z.M. Rittersma, *Sens Actuators A Phys.*, **96**196 (2002).
- [26] H. Farahani, R. Wagiran, M.N. Hamidon, *Sensors*, **15**(5),7881 (2014).
- [27] T.A. Blank, L.P. Eksperiandova, K.N. Belikov, *Sens Actuators, B Chem.* **228**,416 (2016).